Bio-Inspired Structural Colors Produced *via* Self-Assembly of Synthetic Melanin Nanoparticles

Ming Xiao,[†,⊥] Yiwen Li,[‡,⊥] Michael C. Allen,[§] Dimitri D. Deheyn,[§] Xiujun Yue,[‡] Jiuzhou Zhao,[†] Nathan C. Gianneschi,[*,‡] Matthew D. Shawkey,[*,∥] and Ali Dhinojwala[*,†]

[†]Department of Polymer Science, The University of Akron, Akron, Ohio 44325, United States, [‡]Department of Chemistry & Biochemistry, University of California, San Diego, La Jolla, California 92093, United States, [§]Marine Biology Research Division, Scripps Institution of Oceanography, University of California, San Diego, La Jolla, California 92093, United States, and [∥]Department of Biology and Integrated Bioscience Program, The University of Akron, Akron, Ohio 44325, United States. [⊥]These authors (M.X. and Y.L.) contributed equally to this work

ABSTRACT Structural colors arising from interactions of light with submicron scale periodic structures have been found in many species across all taxa, serving multiple biological functions including sexual signaling, camouflage, and aposematism. Directly inspired by the extensive use of self-assembled melanosomes to produce colors in avian feathers, we set out to synthesize and assemble polydopamine-based synthetic melanin nanoparticles in an effort to fabricate colored films. We have quantitatively demonstrated that synthetic melanin nanoparticles have a high refractive index and broad absorption spanning across the UV−visible range, similar to natural melanins. Utilizing a thin-film interference model, we demonstrated the coloration mechanism of deposited films and showed that the unique optical properties of synthetic melanin nanoparticles provide advantages for structural colors over other polymeric nanoparticles (*i.e.*, polystyrene colloidal particles).

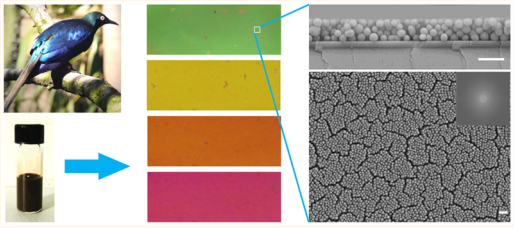

KEYWORDS: structural colors · bio-inspired · biomimicry · polydopamine · melanin

Structural colors, remarkable for their color tunability and resistance to chemical and photo bleaching, have broad applicability in colorimetric sensors,[1−3] full color displays,[4] and photonic pigments.[5] Avian feathers likely possess the highest diversity of structural colors found in nature, with spectral features arising from arrays of melanosomes (submicrometer sized melanin-containing organelles in spherical, rod-like, or disk-like shapes with solid or hollow morphologies[6,7]), such as in the multilayer structures present in the feathers of birds of paradise (*Parotia lawesii*) and in common bronzewings (*Phaps chalcoptera*).[8,9] Other structural color morphologies, including two-dimensional photonic crystal structures, are found in species such as peacocks (*Pavo muticus*) and mallards (*Anas platyrhynchos*).[10,11] The vast array of colors and the ubiquitous use of this approach to coloration and patterning make mimicry of such assemblies highly desirable for synthetic materials. This presents a challenge in nanoscale synthesis of well-defined particles, their self-assembly to generate films, and ultimately in understanding of the underlying principles governing the observed effects.

Melanins, produced in melanosomes, are ubiquitous pigments found in bacteria, fungi, plants, extant animals,[12] and in prehistoric organisms including dinosaurs.[13−16] They are classified as black/brown eumelanins and yellow/reddish pheomelanins based on their precursors.[17] Eumelanins are more intensively studied and have intriguing physicochemical properties, including a monotonic broadband UV−vis absorption, an intrinsic radical center, and electrical and photoconductive properties.[18] Melanins in animal integuments (feathers, hair or skin) are thought to absorb UV radiation to protect living organisms.[17] However, no organism other than birds uses melanosomes to form organized structures for producing colors.[19] Although the physical principles behind structural colors have inspired numerous efforts to generate photonic crystals,[20,21] few have tried to take advantage

* Address correspondence to ngianneschi@ucsd.edu, shawkey@uakron.edu, ali4@uakron.edu.

Received for review February 27, 2015 and accepted May 4, 2015.

Published online May 04, 2015
10.1021/acsnano.5b01298

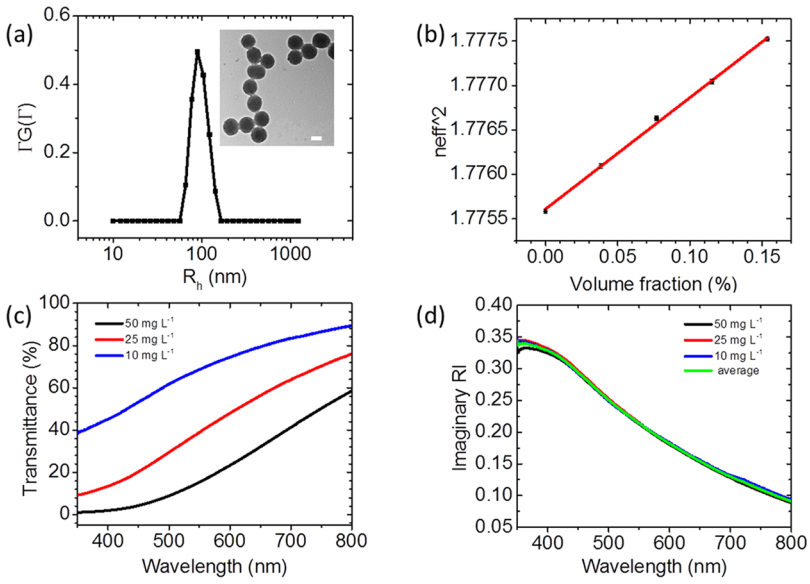

Figure 1. Characterizations of SMNPs. (a) Size distribution of SMNPs, where *y* axis is the contribution of scattered light intensity from different sizes of particles to total light intensity. Inset: TEM image of SMNPs with a scale bar of 100 nm. (b) Square of effective RI of solutions of SMNPs as a function of volume fraction. The slope of the linear fitting is $n_m^2 - n_w^2$. The coefficient of determination for the linear fitting is 0.998. (c) Transmittance spectra for SMNPs solutions at different concentrations (blue, 10 mg L^{-1}; red, 25 mg L^{-1}; black, 50 mg L^{-1}). (d) Imaginary part of the RI as a function of the wavelength. Different colored curves are for each concentration (blue, 10 mg L^{-1}; red, 25 mg L^{-1}; black, 50 mg L^{-1}) and green curve is the averaged value of all three concentrations.

of melanins or melanin-like material to mimic structural colors.[22,23]

Polydopamine (PDA), the most common type of synthetic melanin, has been used extensively in fields as diverse as biology, energy science, sensor development and environmental science,[24] since its first use as a multifunctional coating was inspired by the foot protein in mussels.[25] Although the exact polymerization mechanism for PDA has not yet been clearly elucidated, recent advances have revealed that the physicochemical properties of PDA-based synthetic melanins are generally similar to those of natural melanins,[18,24] giving them promise as photoprotectors,[26] antioxidants,[27] semiconductors,[28] and biomedical materials.[29]

Recently, Kohri *et al.*[22] used different sizes of PDA particles to spray coat films of different colors. In this case, colors were mostly generated due to scattering phenomena. Wu *et al.*[23] fabricated colored reflectors by placing a thin PDA film on top of a thick layer of amorphous PDA particles that served as a strong absorbing layer. However, despite their prevalence in the natural world, and obvious advantages in developing the diversity of colors produced by birds in particular, direct bio-inspired coloration from ordered structures of PDA particles has not yet been reported. In addition, what advantages PDA particles may offer relative to common polymeric particles in terms of structural coloration has not yet been elucidated. Here, inspired by structural coloration arising from assembled melanosomes in avian feathers, we have prepared and assembled synthetic melanin nanoparticles (SMNPs, Figure 1) to construct structurally colored films using an evaporative process. We have measured the complex refractive index (RI) of SMNPs and have established a thin-film interference model that explains the origin of observed colors. The SMNPs and their self-assembly into films provide an approach for mimicking the vibrant colors found in avian feathers with a wide range of potential applications in the design of optical devices, functional coatings, and biocompatible products.

RESULTS AND DISCUSSIONS

Inspired by the dimension of natural melanosomes in structurally colored feathers (*e.g.*, the diameter of rod-like shaped melanosomes is 120−170 nm for ducks[11] and 140−180 nm for peacocks[10]), we have fabricated SMNPs with an average diameter of 146 ± 15 nm as measured *via* transmission electron microscopy (TEM) (Figure 1a). Dynamic light scattering (DLS) measurements are consistent with TEM data, revealing that SMNPs in solution have a narrow distribution with an average diameter of 184 nm. Measurements of effective RI of solutions of aqueous SMNPs (n_{eff}^2) as a function of volume fractions of SMNPs showed a near perfect linear relationship (Figure 1b), which matches the Drude model,[30] $n_{eff}^2 = V_m n_m^2 + (1 - V_m) n_w^2$. The real part of the RI of SMNPs was calculated to be 1.741 ± 0.001 at 589 nm (eq S1, Supporting Information). These calculations reveal the value of RI for synthetic melanin is appreciably higher than most synthetic polymers (~1.4−1.6 at 589 nm).[31] The imaginary component of RI was

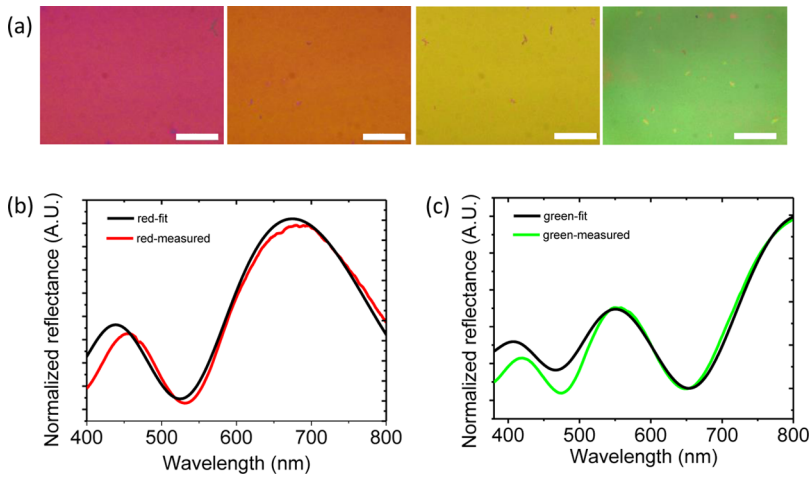

Figure 2. Optical characterizations of SMNP films. (a) Optical images of colored films. The red and orange colors are from different regions of the film in Supporting Information Figure S1b, and the yellow and green colors are from different locations of the film in Supporting Information Figure S1c. Scale bars: 100 μm. (b) Measured (red curve) and modeled (black curve) reflectance spectra of red film in (a). (c) Measured (green curve) and modeled (black curve) reflectance spectra of green film in (a).

calculated (eqs S4 and S5, Supporting Information) using the transmittance (or absorption) data for the solutions of SMNPs. (Figure 1c). As expected from theory, we obtained similar values for the imaginary part of the RI of SMNPs for all the three concentrations (10, 25, and 50 mg L^{-1}), with a small discrepancy for the values below 400 nm, probably due to the measurement errors at short wavelength from low transmittance. Previous reports describe experimental and modeling data suggesting a range of 1.65−2.0 for RI of natural melanins, although much debate remains concerning the exact value.[10,11,32] Certainly, our measurements show that both real and imaginary parts of RI for SMNPs are similar to those reported for natural melanins[32] with the broad absorption of light by SMNPs in the UV−visible region being comparable to that of natural melanin.[17]

We prepared colored films of SMNPs using a vertical evaporation-based self-assembly approach.[33] Subsequently, a wide range of colors (red, orange, yellow, and green) was obtained by evaporating 0.6 and 1.0 mg mL^{-1} solutions of SMNPs at an evaporation rate of 0.50−0.55 mm h^{-1} (Figure 2a). The concentration of the solution was important for controlling the uniformity of the films with separate strips of colors running perpendicular to the evaporation front formed at low concentration, and gray or black films formed at high concentrations (Supporting Information Figure S1). An inherent feature of this approach to the assembly of ordered films is that the concentration changes during evaporation, making it difficult to obtain one uniform color across the entire 1 × 1 cm^2 area of the sample. However, the uniformity over 1 mm was sufficient for both optical characterization and cross-sectional scanning electron microscopy (SEM) analyses.

The reflectance spectra for red and green films show two peaks in the visible region with primary peak positions at 675 and 550 nm corresponding to the red and green color, respectively (Figure 2b,c). As a control, the reflectance spectra for blank silicon wafers show no discernible peak and very high reflectance at short wavelengths, demonstrating that the colors observed for films of SMNPs are not caused by the silicon substrate (Supporting Information Figure S2). Furthermore, hyperspectral images (Figure 3) show that the green color has a purity of 84%, with red color purity as high as 95% for a scanning area of 0.05 × 0.1 mm^2. The reflectance spectra measured using hyperspectral imaging are very similar to those obtained using the microspectrophotometer, complementarily confirming the uniformity of the films in terms of colors.

SEM cross-sectional images of regions of the films associated with green and red colors revealed thicknesses measured to be approximately 338 ± 9 and 444 ± 15 nm, respectively (Figure 4). Top view SEM images of the films showed close-packed SMNPs lacking long-range crystalline order; an observation confirmed by analysis of the two-dimensional Fourier power spectra (Figure 4c,d). In each case, the films have small and evenly distributed cracks, due to shrinkage during the drying process. These cracks do not affect the color measurements because the measured spot size (10 × 10 μm^2 for microspectrophotometer measurements, 0.05 × 0.1 mm^2 for hyperspectral imaging) is on a longer length-scale than crack widths. We further modeled the reflectivity data using a four-layer thin-film interference model (air plus film of SMNPs plus silicon oxide plus silicon. For details, see Experimental Section). We used an interactive method on the packing density of SMNPs in the film to obtain the best match with measured reflectance spectra, with the best fitting packing density of 54% for red film and 56% for green film (Figure 2b,c). The obtained optimal packing density is reasonable, and lower than the

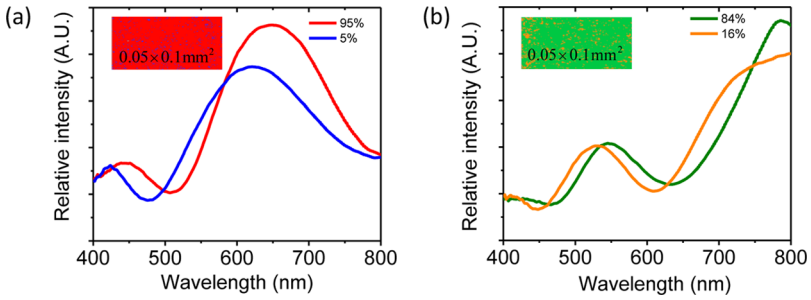

Figure 3. Hyperspectral analysis of (a) red and (b) green SMNP films. In each case, two distinct spectra (shown with different color codes) contributed to the color measured in specular reflectance. Each spectrum corresponded to a different pixel percent of the scanned area, and the low-occurrence spectrum always appeared randomly scattered across the scanned area (see insets).

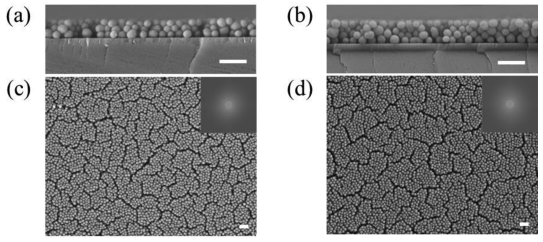

Figure 4. SEM images of structure of SMNP films. (a and b) SEM cross-sectional images of the red film and green film, respectively; (c and d) top view SEM images of the red and green films, respectively. The insets in panels (c) and (d) correspond to 2D Fourier power spectra. Scale bars: 500 nm.

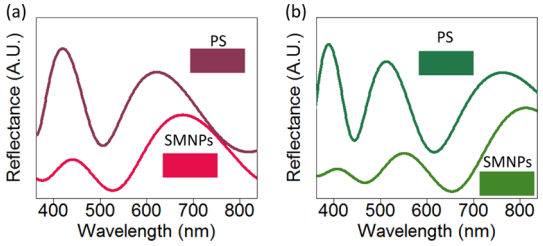

Figure 5. Modeled reflectance spectra for films of PS nanoparticle and SMNPs. The colors of the curves are colored with RGB standards using "rgb2spec" in Pavo package of R.[47] (a) The thickness of nanoparticle layer is 338 nm; peak area ratio between the shorter wavelength peak (420 nm) and the longer wavelength peak (620 nm) is 0.70 for PS;, while peak area ratio between the shorter wavelength peak (440 nm) and the longer wavelength peak (680 nm) is 0.11 for SMNPs. (b) The thickness of nanoparticle layer is 444 nm; peak area ratio between the shorter wavelength peak (390 nm) and the longer wavelength peak (510 nm) is 0.64 for PS, while peak area ratio between the shorter wavelength peak(405 nm) and the longer wavelength peak (550 nm) is 0.22 for SMNPs.

theoretically maximum random closed packing density of 63.4%.[34] Small discrepancies at shorter wavelengths may be due to the dispersion of the real part of the RI of SMNPs in the visible range. The optical model of red and green colors (longest and shortest wavelengths we achieved) shows that the variation of colors is primarily due to differences in the thickness of the SMNPs layers. The color generated here is not directly related to the particle size. The particle size influences the packing density, indirectly affecting the refractive index and the color produced by thin-film interference, but this effect is beyond the scope of this study.

Although self-assembly of colloidal nanoparticles to generate color has been well documented,[35,36] most established systems use polymeric particles such as polystyrene (PS) and poly(methyl methacrylate) (PMMA), which usually display negligible absorption of light in the visible range. However, the broad absorption spectrum of SMNPs is important for generating more saturated colors. In recent studies it has been shown that adding carbon black nanoparticles reduces incoherent scattering and enhances color saturation.[37,38] We simulated the reflectance spectra (Figure 5) for films consisting of PS nanoparticles with similar packing density and thickness as the red and green films, as showed in Figure 2a. We used the following dispersion equation for real part of the RI of PS.[39]

$$n = 1.573 + \frac{3108}{\lambda^2} + \frac{3.478 \times 10^8}{\lambda^4} \qquad (1)$$

In eq 1, λ is the wavelength (nm). The imaginary part of the RI of PS is ~0, due to negligible absorption between 400 and 800 nm.[39] Both spectra for SMNPs and PS particles have two peaks in the visible range. Interestingly, the two peaks for PS films have similar intensities (peak area ratio = 0.64−0.70), while the peak at shorter wavelength is much attenuated, reaching only 11% of the area of the peak at longer wavelength for the red film of SMNPs and 22% for the green film of SMNPs.

SMNPs have unique absorption patterns (high absorption at short wavelengths and low absorption at long wavelengths) that enhance color purity and provide UV-protection. Additionally, RI of SMNPs is much higher than that of most polymers, providing a relatively high RI contrast necessary for the design of highly sensitive colorimetric sensor.[40] Relative to some reported metal oxide nanoparticles with even higher RI used to create structural colors,[41] bio-inspired SMNPs potentially are less toxic, more biodegradable, and are inherently biocompatible.[42] Moreover, these biomimetic structural colors can be directly obtained *via* assembly of SMNPs in aqueous solution, potentially

offering a route toward a biocompatible structural color palette.

CONCLUSIONS

We have demonstrated a biomimetic approach for generating structural colors *via* evaporation-induced self-assembly of well-defined SMNPs. We have shown that SMNPs possess a high RI and broad absorption spanning the UV−visible range, similar to natural melanin, providing the necessary contrast for structural colors. Colors ranging from green to red were produced by evaporation-based self-assembly of these nanoparticles. Controlling the thickness of the assembled nanoparticles produced different colors, which were successfully predicted using a thin-film interference model. In addition, SMNPs can be manufactured in large quantities and are biocompatible. Our results show the unique advantage of using melanosomes to generate colors found in the animal kingdom and also offer numerous new opportunities toward multifunctional photonic devices and biocompatible products. In the future, increased control of the self-assembly process will be investigated as a necessity in obtaining large-scale films capable of producing the full color spectrum. Ongoing studies will explore alternative assembly procedures and utilize analogous SMNPs with various morphologies and compositions.

EXPERIMENTAL SECTION

Synthesis and Characterization of SMNPs. The SMNPs were synthesized through the oxidation and self-polymerization of dopamine molecules in a solution consisting of water, ethanol and ammonia at room temperature, which is modified from the previous literature.[42] Although many parameters could affect the final size of the SMNPs, we optimized the required size by tuning the molar ratio of ammonia and dopamine hydrochloride. Typically, to synthesize SMNPs with average diameter of ~146 nm, 50 mL of deionized water and 20 mL of ethanol were fully mixed with 1.2 mL of ammonia aqueous solution (28−30%) under stirring at room temperature for about 1 h. A 5 mL dopamine hydrochloride aqueous solution (4 mg/mL) was quickly injected into this solution. It was observed that the solution color turned to pale yellow immediately and then gradually changed to black after 1 h. After 18 h, the targeted SMNPs were separated by centrifugation and washing with deionized water thrice. All chemicals are purchased from Sigma-Aldrich. We characterized the size of SMNPs in solution by DLS measurements using a BI−HV Brookhaven instrument with a 633 nm solid-state laser (Brookhaven Instruments Corp.). DLS data were analyzed using CONTIN software to determine the hydrodynamic diameter. The size of the nanoparticles was also confirmed using a JEM-1230 transmission electron microscope (TEM) (JEOL Ltd.) after drying.

Evaporation-Based Assembly. Silicon wafers (Silicon, Inc.) were cut into 1 × 1 cm^2 and ultrasonicated in 2 wt % sodium dodecyl sulfate (Sigma) solution for 30 min, followed by washing with deionized water for 30 min, and a final rinse using acetone for 30 min. After a drying step, the silicon substrates were subjected to a 5 min air plasma treatment (Harrick Plasma, PDC-32G). One milliliter of SMNPs in water of a known concentration was ultrasonicated for 15 min and placed into a plastic cuvette (Brandtech). A clean silicon wafer was held vertically in the solution at 60 °C until all the water evaporated. A separate cuvette filled with water was used to monitor the evaporation rate (expressed as change in height (mm) per unit hour). We also measured the thickness of the top thin silica layer of bare silicon wafer using a multiple wavelength mode ellipsometer (J.A. Woollam Corp.) before evaporative deposition of SMNPs.

Characterization of the SMNP Film. Optical images of deposited films were taken using an Olympus BX51microscope (Olympus Corp.). CRAIC AX10 UV−visible-NIR microspectrophotometer (MSP) (CRAIC Technologies, Inc., a 15× objective, range 400−800 nm) was used to measure the normal reflectance spectra of deposited films of SMNPs at various locations that showed uniform colors. We normalized the reflectance with respect to a white standard of high density Teflon tape (TaegaTech).

To characterize the purity of the color and the spectral homogeneity of the film at a fine spatial scale, we performed measurements using a PARISS hyperspectral imaging system (LightForm, Inc.) mounted on a Nikon 80i microscope outfitted with a monochrome Retiga 2000DC CCD camera (QImaging). The system was radiometrically calibrated with accuracy better than 2 nm. The film was analyzed under specular reflectance (with a tungsten halogen white light, neutrally color balanced using a Nikon NCB11 filter) using a 100× air objective, capturing spectra (400−800 nm) from all digital pixels of an area of 0.05 × 0.1 mm^2. The reflectance spectra were then normalized with respect to a standard silver mirror (ThorLabs, Inc.) and smoothed with a moving average of 3 as recommended by the vendor. For relative comparison of spectral intensity, all acquisition parameters were kept the same from one mapped area to the other. All spectra from one individual area showing >99% closeness of fit were identified by one single representative spectrum. For data presentation (Figure 3), we show the mapping of the different spectra using artificial color coding. We display the normalized spectra corresponding to the color coded map and show the ratio of the number of pixels of the mapped area that is associated with each spectrum.

For electron microscopy, the top-view and cross-sectional structures were obtained using SEM (JEOL-7401, JEOL Ltd.) after silver sputter coating using a K575X turbo sputter coater (Emitech). To measure the thickness of the deposited film, we cut the SMNPs deposited wafer into half and vertically aligned the cut edge for SEM imaging. We used ImageJ (http://imagej.nih.gov/ij/) to measure the thickness of the melanin film from the SEM images.

Optical Modeling. A matrix method[43,44] was used to calculate reflectivity data for a four-layer thin film model, which consists of a layer of air, a randomly packed film of SMNPs, a silicon oxide layer, and a thick silicon substrate. The thickness of SMNPs film was measured by analyzing cross-sectional SEM images (Figure 4a,b). The silicon oxide layer was 119 ± 3 nm thick measured using ellipsometry before depositing the melanin films, which was consistent with the value of 121 ± 6 nm measured using the SEM cross-sectional images. The RI values of silicon oxide and silicon are 1.458 and 3.973, respectively.[45,46]

Conflict of Interest: The authors declare no competing financial interest.

Supporting Information Available: Additional information contains two parts: (1) the measurements of the complex RI and (2) supporting figures S1−S2, optical images, and reflectance spectrum of wafer. The Supporting Information is available free of charge on the ACS Publications website at DOI: 10.1021/acsnano.5b01298.

Acknowledgment. Thank you to Boxiang Wang for discussions concerning the thin-film model and refractive index measurements. We acknowledge Nita Sahai for providing the use of a refractometer. Thank you to Branislav Igic, Liliana D'Alba, Bill Hsiung, Daphne Fecheyr-Lippens and Jenny Peteya for helpful discussion and comments on the manuscript. We

acknowledge financial support from NSF DMR-1105370 (A.D.), AFOSR FA9550-13-1-0222, HFSP grant RGY-0083 and NSF Ear-1251895 (M.D.S.), AFOSR MURI BioPaints FA9550-10-1-0555 and BioOptics FA 9550-09-1-0669 (D.D.D.), and AFOSR PECASE (FA9550-11-1-0105) (N.C.G.).

REFERENCES AND NOTES

1. Holtz, J. H.; Asher, S. A. Polymerized Colloidal Crystal Hydrogel Films as Intelligent Chemical Sensing Materials. *Nature* **1997**, *389*, 829–832.
2. Kim, E.; Kim, S. Y.; Jo, G.; Kim, S.; Park, M. J. Colorimetric and Resistive Polymer Electrolyte Thin Films for Real-Time Humidity Sensors. *ACS Appl. Mater. Interfaces* **2012**, *4*, 5179–5187.
3. Chan, E. P.; Walish, J. J.; Thomas, E. L.; Stafford, C. M. Block Copolymer Photonic Gel for Mechanochromic Sensing. *Adv. Mater.* **2011**, *23*, 4702–4706.
4. Arsenault, A. C.; Puzzo, D. P.; Manners, I.; Ozin, G. A. Photonic-Crystal Full-Colour Displays. *Nat. Photonics* **2007**, *1*, 468–472.
5. Park, J. G.; Kim, S. H.; Magkiriadou, S.; Choi, T. M.; Kim, Y. S.; Manoharan, V. N. Full-Spectrum Photonic Pigments with Non-Iridescent Structural Colors through Colloidal Assembly. *Angew. Chem., Int. Ed.* **2014**, *53*, 2899–2903.
6. Maia, R.; Rubenstein, D. R.; Shawkey, M. D. Key Ornamental Innovations Facilitate Diversification in an Avian Radiation. *Proc. Natl. Acad. Sci. U.S.A.* **2013**, *110*, 10687–10692.
7. Shawkey, M. D.; D'Alba, L.; Xiao, M.; Schutte, M.; Buchholz, R. Ontogeny of an Iridescent Nanostructure Composed of Hollow Melanosomes. *J. Morphol.* **2014**, *276*, 378–384.
8. Wilts, B. D.; Michielsen, K.; De Raedt, H.; Stavenga, D. G. Sparkling Feather Reflections of a Bird-Of-Paradise Explained by Finite-Difference Time-Domain Modeling. *Proc. Natl. Acad. Sci. U.S.A.* **2014**, *111*, 4363–4368.
9. Xiao, M.; Dhinojwala, A.; Shawkey, M. Nanostructural Basis of Rainbow-Like Iridescence in Common Bronzewing *Phaps chalcoptera* Feathers. *Opt. Express* **2014**, *22*, 14625–14636.
10. Zi, J.; Yu, X. D.; Li, Y. Z.; Hu, X. H.; Xu, C.; Wang, X. J.; Liu, X. H.; Fu, R. T. Coloration Strategies in Peacock Feathers. *Proc. Natl. Acad. Sci. U.S.A.* **2003**, *100*, 12576–12578.
11. Eliason, C. M.; Shawkey, M. D. A Photonic Heterostructure Produces Diverse Iridescent Colours in Duck Wing Patches. *J. R. Soc. Interface* **2012**, *9*, 2279–2289.
12. Prota, G. *Melanins and Melanogenesis*; Academic Press: San Diego, CA, 1992.
13. Li, Q.; Clarke, J. A.; Gao, K.-Q.; Zhou, C.-F.; Meng, Q.; Li, D.; D'Alba, L.; Shawkey, M. D. Melanosome Evolution Indicates a Key Physiological Shift within Feathered Dinosaurs. *Nature* **2014**, *507*, 350–353.
14. Li, Q.; Gao, K.-Q.; Meng, Q.; Clarke, J. A.; Shawkey, M. D.; D'Alba, L.; Pei, R.; Ellison, M.; Norell, M. A.; Vinther, J. Reconstruction of Microraptor and the Evolution of Iridescent Plumage. *Science* **2012**, *335*, 1215–1219.
15. Lindgren, J.; Sjövall, P.; Carney, R. M.; Uvdal, P.; Gren, J. A.; Dyke, G.; Schultz, B. P.; Shawkey, M. D.; Barnes, K. R.; Polcyn, M. J. Skin Pigmentation Provides Evidence of Convergent Melanism in Extinct Marine Reptiles. *Nature* **2014**, *506*, 484–488.
16. Clarke, J. A.; Ksepka, D. T.; Salas-Gismondi, R.; Altamirano, A. J.; Shawkey, M. D.; D'Alba, L.; Vinther, J.; DeVries, T. J.; Baby, P. Fossil Evidence for Evolution of the Shape and Color of Penguin Feathers. *Science* **2010**, *330*, 954–957.
17. Simon, J. D.; Peles, D. N. The Red and the Black. *Acc. Chem. Res.* **2010**, *43*, 1452–1460.
18. d'Ischia, M.; Napolitano, A.; Ball, V.; Chen, C.-T.; Buehler, M. J. Polydopamine and Eumelanin: from Structure–Property Relationships to a Unified Tailoring Strategy. *Acc. Chem. Res.* **2014**, *47*, 3541–3550.
19. Hill, G. E.; McGraw, K. J. *Bird Coloration: Function and Evolution*; Harvard University Press: Cambridge, MA, 2006; Vol. 2.
20. Zhao, Y.; Xie, Z.; Gu, H.; Zhu, C.; Gu, Z. Bio-Inspired Variable Structural Color Materials. *Chem. Soc. Rev.* **2012**, *41*, 3297–3317.
21. Khudiyev, T.; Dogan, T.; Bayindir, M. Biomimicry of Multifunctional Nanostructures in the Neck Feathers of Mallard (*Anas platyrhynchos L.*) Drakes. *Sci. Rep.* **2014**, *4*.
22. Kohri, M.; Nannichi, Y.; Taniguchi, T.; Kishikawa, K. Biomimetic Non-Iridescent Structural Color Materials from Polydopamine Black Particles That Mimic Melanin Granules. *J. Mater. Chem. C* **2015**, *3*, 720–724.
23. Wu, T.-F.; Hong, J.-D. Dopamine-Melanin Nanofilms for Biomimetic Structural Coloration. *Biomacromolecules* **2015**, *16*, 660–666.
24. Liu, Y.; Ai, K.; Lu, L. Polydopamine and its Derivative Materials: Synthesis and Promising Applications in Energy, Environmental, and Biomedical Fields. *Chem. Rev.* **2014**, *114*, 5057–5115.
25. Lee, H.; Dellatore, S. M.; Miller, W. M.; Messersmith, P. B. Mussel-Inspired Surface Chemistry for Multifunctional Coatings. *Science* **2007**, *318*, 426–430.
26. Corani, A.; Huijser, A.; Gustavsson, T.; Markovitsi, D.; Malmqvist, P.-Å.; Pezzella, A.; d'Ischia, M.; Sundström, V. Superior Photoprotective Motifs and Mechanisms in Eumelanins Uncovered. *J. Am. Chem. Soc.* **2014**, *136*, 11626–11635.
27. Ju, K.-Y.; Lee, Y.; Lee, S.; Park, S. B.; Lee, J.-K. Bioinspired Polymerization of Dopamine to Generate Melanin-Like Nanoparticles Having an Excellent Free-Radical-Scavenging Property. *Biomacromolecules* **2011**, *12*, 625–632.
28. McGinness, J.; Corry, P.; Proctor, P. Amorphous Semiconductor Switching in Melanins. *Science* **1974**, *183*, 853–855.
29. Bettinger, C. J.; Bruggeman, J. P.; Misra, A.; Borenstein, J. T.; Langer, R. Biocompatibility of Biodegradable Semiconducting Melanin Films for Nerve Tissue Engineering. *Biomaterials* **2009**, *30*, 3050–3057.
30. Sihvola, A. H. *Electromagnetic Mixing Formulas and Applications*; Institution of Engineering and Technology United Kingdom: London, 1999.
31. Mark, J. E. *Physical Properties of Polymers Handbook*, 2nd ed.; Springer: New York, NY, 2007.
32. Stavenga, D. G.; Leertouwer, H. L.; Hariyama, T.; De Raedt, H. A.; Wilts, B. D. Sexual Dichromatism of the Damselfly *Calopteryx japonica* Caused by a Melanin-Chitin Multilayer in the Male Wing Veins. *PLoS One* **2012**, *7*, e49743.
33. Hatton, B.; Mishchenko, L.; Davis, S.; Sandhage, K. H.; Aizenberg, J. Assembly of Large-Area, Highly Ordered, Crack-Free Inverse Opal Films. *Proc. Natl. Acad. Sci. U.S.A.* **2010**, *107*, 10354–10359.
34. Song, C.; Wang, P.; Makse, H. A. A Phase Diagram for Jammed Matter. *Nature* **2008**, *453*, 629–632.
35. Cong, H.; Cao, W. Thin Film Interference of Colloidal Thin Films. *Langmuir* **2004**, *20*, 8049–8053.
36. Galisteo-López, J. F.; Ibisate, M.; Sapienza, R.; Froufe-Pérez, L. S.; Blanco, Á.; López, C. Self-Assembled Photonic Structures. *Adv. Mater.* **2011**, *23*, 30–69.
37. Forster, J. D.; Noh, H.; Liew, S. F.; Saranathan, V.; Schreck, C. F.; Yang, L.; Park, J. G.; Prum, R. O.; Mochrie, S. G.; O'Hern, C. S. Biomimetic Isotropic Nanostructures for Structural Coloration. *Adv. Mater.* **2010**, *22*, 2939–2944.
38. Takeoka, Y.; Yoshioka, S.; Takano, A.; Arai, S.; Nueangnoraj, K.; Nishihara, H.; Teshima, M.; Ohtsuka, Y.; Seki, T. Production of Colored Pigments with Amorphous Arrays of Black and White Colloidal Particles. *Angew. Chem., Int. Ed.* **2013**, *52*, 7261–7265.
39. Ma, X.; Lu, J. Q.; Brock, R. S.; Jacobs, K. M.; Yang, P.; Hu, X.-H. Determination of Complex Refractive Index of Polystyrene Microspheres from 370 to 1610 nm. *Phys. Med. Biol.* **2003**, *48*, 4165.
40. Xu, X.; Goponenko, A. V.; Asher, S. A. Polymerized poly-HEMA photonic crystals: pH and ethanol sensor materials. *J. Am. Chem. Soc.* **2008**, *130*, 3113–3119.
41. He, L.; Janner, M.; Lu, Q.; Wang, M.; Ma, H.; Yin, Y. Magnetochromatic Thin-Film Microplates. *Adv. Mater.* **2015**, *27*, 86–92.
42. Liu, Y.; Ai, K.; Liu, J.; Deng, M.; He, Y.; Lu, L. Dopamine-Melanin Colloidal Nanospheres: An Efficient Near-Infrared Photothermal Therapeutic Agent for *in Vivo* Cancer Therapy. *Adv. Mater.* **2013**, *25*, 1353–1359.

43. Azzam, R. M.; Bashara, N. M. *Ellipsometry and Polarized Light*; North-Holland: Amsterdam, The Netherland, 1977.
44. Jellison, G., Jr Data Analysis for Spectroscopic Ellipsometry. *Thin Solid Films* **1993**, *234*, 416–422.
45. Malitson, I. Interspecimen Comparison of the Refractive Index of Fused Silica. *J. Opt. Soc. Am.* **1965**, *55*, 1205–1208.
46. Aspnes, D.; Studna, A. Dielectric Functions and Optical Parameters of Si, Ge, GaP, GaAs, GaSb, InP, InAs, and InSb from 1.5 to 6.0 eV. *Phys. Rev. B* **1983**, *27*, 985–1009.
47. Maia, R.; Eliason, C. M.; Bitton, P. P.; Doucet, S. M.; Shawkey, M. D. Pavo: An R Package for the Analysis, Visualization and Organization of Spectral Data. *Methods Ecol. Evol.* **2013**, *4*, 906–913.